SYNTHESIS AND CHARACTERIZATION OF HEXAAMMINE NICKEL HALIDES INTENDED FOR SOLID-STADE HYDROGEN

Mirzeta Saletović [1], Filip Brleković [2*], Nina Mašić [1], Amila Jusufović [1], Amina Djedović [1], Katarina Mužina [2], Stanislav Kurajica [2]

[1] *University of Tuzla, Faculty of Natural Science and Mathematics, Department of Chemisty, Urfeta Vejzafića 4, 75 000 Tuzla, Bosnia and Herzegovina*

[2] *University of Zagreb, Faculty of Chemical Engineering and Technology, Marulićev trg 19, HR 10000 Zagreb, Croatia*

*E-mail of corresponding author: fbrlekovi@fkit.unizg.hr

Abstract: *Hydrogen is a versatile energy carrier but its storing is challenging. For that reason, alternative hydrogen storage approaches are being intensively researched. Solid state storing of hydrogen in the form of ammines offers certain advantages, such as high storage capacity and relatively low toxicity. Therefore, in this work hexaammine complexes of nickel chloride and nickel bromide were prepared and investigated. $Ni(NH_3)_6Cl_2$ and $Ni(NH_3)_6Br_2$, were obtained by precipitation synthesis. The prepared complexes were characterized by scanning electron microscopy (SEM), energy dispersive X-ray spectroscopy (EDS), X-ray powder diffraction (PXRD), Fourier transform infrared spectroscopy (FTIR), thermo-gravimetric analysis (TGA) and differential scanning calorimetry (DSC). The prepared particles are polydisperse, agglomerated and show a characteristic octahedral morphology. The samples consist solely of pure, well-crystalline, corresponding hexaamine complexes. $Ni(NH_3)_6Br_2$ shows somewhat weaker nitrogen bonds with the central cation and weaker hydrogen bonds with halogen compared to $Ni(NH_3)_6Cl_2$. Thermal analyses have shown that under the experimental conditions used, ammonia is released from $Ni(NH_3)_6Cl_2$ in three stages, while in the case of $Ni(NH_3)_6Br_2$, decomposition occurs in two stages. This difference is a consequence of the kinetic parameters of the desorption process. The maximum of the first stage of desorption occurs for the $Ni(NH_3)_6Cl_2$ sample at a slightly lower temperature than for the $Ni(NH_3)_6Br_2$ sample, which is attributed to thermodynamic factors.*

Keywords: *ammonia chemical storage, hexaammine nickel(II) chloride, hexaammine nickel(II) bromide, thermal analysis*

Received: 28.08.2025. / Accepted: 10.12.2025.
Published online: 18.12.2025.

Original scientific paper

1. INTRODUCTION

The greenhouse effect has driven significant development of renewable energy sources. However, renewable energy sources such as sun and wind are intermittent by nature and their power generation is unpredictable and cannot be directly controlled by power grid operators as traditional power sources. That could impair electro energetic system stability by causing supply-demand imbalances and introducing fluctuations in voltage and frequency, which can lead to instability and blackouts. This problem has been addressed by development of energy storage systems able to capture excess energy when production is high and release it when it is low (Müller 2021). In such manner power supply and demand could be balanced, power grid stability ensured and, last but not least, greater renewable energy sources utilization enabled. There are several approaches to this problem, one of the most notable being energy storage in the form of hydrogen, as hydrogen is characterized by a high gravimetric energy density (Klopčić 2023). In this way, energy obtained from renewable sources can be used to produce hydrogen via water electrolysis; the resulting hydrogen is stored and, when needed, converted back into electrical energy through oxidation in a fuel cell (Sørensen 2005). It sounds simple, but storing compressed or liquefied hydrogen comes with numerous technical and safety challenges. Some of the technical problems are the need for tanks for compressed hydrogen that can withstand very high pressures or tanks for liquified hydrogen operating at very low temperatures. Also, hydrogen atoms diffuse into the metal structure, which causes metal embrittlement which could cause failure under tensile stress. On the other hand, main safety challenges are risks of explosion and fire. For this reason, materials that enable hydrogen storage in the solid state are being intensively researched (Kojima 2020). The synthesis, understanding, and development of these materials are crucial for further progress in sustainable systems for energy production, storage, and delivery (Mandal 2009).

Although metal hydrides were initially recognized as suitable materials for hydrogen storage in solid state (von Colbe 2019), hydrogen can also be stored in the form of ammonia, which can in this context be produced through an electrochemical process (Aziz 2020). Furthermore, ammonia is easier to liquefy, store, and transport; it has a higher autoignition temperature than hydrogen and can be relatively easily converted back into hydrogen (Kojima 2020), (Freeman 2023), or used directly in suitable fuel cells (Ni 2008). However, ammonia is toxic

and produces harmful gases upon oxidation, which is why solid-state storage of ammonia is also being explored – primarily in the form of complex metal ammine salts with halogen elements (Reardon 2012). In these complex salts, six NH_3 ligands coordinate around a metal cation to form an octahedron (**Figure 1**) (Liu 2004):

$$MXm+n\mathrm{NH_3} \rightarrow M(\mathrm{NH_3})_n\mathrm{X}_m \quad (1)$$

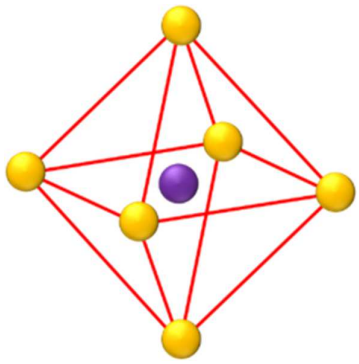

Figure 1. *Structural model of the hexaammine complex $M(NH_3)_6^{2+}$ (the metal ion is shown as a purple sphere, while the yellow spheres represent NH_3 molecules).*

Although this is an indirect method of storage, storing hydrogen in the form of ammines offers certain advantages, such as high storage capacity and relatively low toxicity (Klerke 2008). The most thoroughly studied compound for this purpose is hexaammine magnesium(II) chloride, $Mg(NH_3)_6Cl_2$ (Jacobsen 2007). However, the literature also reports investigations on hexaammine manganese(II) chloride (Reardon 2012), as well as hexaammine nickel(II) chloride, bromide, and iodide (Breternitz, 2016). In addition, solid solutions such as $Mg_{1-x}Mn_x(NH_3)_6Cl_2$ (Berdyeva 2020) and $Ba_{1-x}Sr_x(NH_3)_6Cl_2$ (Bialy 2015) have been studied. Further research has been conducted on solid solutions of the type $Ca(NH_3)_6Cl_{2-x}Br_x$, $Sr(NH_3)_6Cl_{2-x}Br_x$, and $Sr(NH_3)_6Cl_{2-x}I_x$. These studies have shown the potential for tuning the ammonia sorption process (Liu 2004), (Hodorowicz 1982).

Key advantages of hexamine nickel(II) halides as hydrogen storage compounds are safe solid-state form, high storage density and fast release kinetics. In comparison to some other hexamine metal halides they require lower decomposition temperatures, have good air stability and rapid room temperature regeneration cycles, making hexamine nickel(II) halides potential candidates for mobile applications. (Straub 2023) The most fruitful research on hexamine nickel(II) halides is that of Breternitz et al., (Breternitz 2016) classifying those compounds among most promising for ammonia storage.

Therefore, the aim of this work was to synthesize nickel ammine complexes – hexaammine nickel(II) chloride, $[Ni(NH_3)_6]Cl_2$, and hexaammine nickel(II) bromide, $[Ni(NH_3)_6]Br_2$ – and to characterize their morphology, phase and chemical composition, thermal stability, and decomposition behaviour.

2. MATERIALS AND METHODS

2.1. Synthesis of Hexaammine nickel(II) Chloride, $[Ni(NH_3)_6]Cl_2$

The following chemicals were used for the synthesis: nickel(II) chloride hexahydrate, p.a., Centrohem, Stara Pazova, Serbia; ammonia, 25% aqueous solution, p.a., GRAM-MOL, Zagreb, Croatia; and acetone, LACH NER, Zagreb, Croatia. Nickel(II) chloride hexahydrate was first dissolved in distilled water, and the mixture was heated on a hot plate until the crystals were completely dissolved. During this process, dissociation occurs, resulting in the formation of the green hexaaquanickel(II) complex and chloride anions:

$$Ni(H_2O)_6Cl_2 \rightarrow Ni(H_2O)_6^{2+} + 2Cl^- \quad (2)$$

The ammonia solution was added slowly, dropwise and with continuous stirring, to the hot aqueous solution of nickel(II) chloride hexahydrate. Slow addition of ammonia is necessary to ensure complete reaction. Since ammonia forms a stronger bond with nickel than water does, it displaces the water molecules from the complex, resulting in the formation of the purple hexaammine nickel(II) complex:

$$Ni(H_2O)_6^{2+} + 6(NH_3) \rightarrow Ni(NH_3)_6^{2+} + 6H_2O \quad (3)$$

The resulting solution was left at room temperature for approximately 30 minutes with occasional stirring. It was then placed in an ice bath prepared from crushed ice and water. After a short period, precipitation of the purple hexaammine nickel(II) chloride occurred:

$$Ni(NH_3)_6^{2+} + 2Cl^- \rightarrow [Ni(NH_3)_6]Cl_2 + 6H_2O \qquad (4)$$

The precipitated crystals were filtered using a Büchner funnel connected to a vacuum pump and washed first with concentrated ammonia, followed by acetone. The product was then air-dried under reduced pressure.

2.2. Synthesis of Hexaamminenickel(II) Bromide, $[Ni(NH_3)_6]Br_2$

The following chemicals were used for the synthesis: nickel(II) sulfate, p.a., Hemos, Belgrade, Serbia; sodium hydroxide, p.a., GRAM-MOL, Zagreb, Croatia; ammonia, 25 % aqueous solution, p.a., GRAM-MOL, Zagreb, Croatia; and hydrobromic acid, Acros, Geel, Belgium. Nickel(II) sulfate was dissolved in water and precipitated with a sodium hydroxide solution, yielding green nickel(II) hydroxide:

$$NiSO_4 + 2NaOH \rightarrow Ni(OH)_2 + Na_2SO_4 \qquad (5)$$

The precipitate was filtered and washed with water until no sulfate ions were detected (tested with $BaCl_2$). The washed precipitate was then transferred to a porcelain dish and dissolved in concentrated hydrobromic acid, resulting in the formation of nickel(II) bromide:

$$Ni(OH)_2 + {}_2HBr \rightarrow NiBr_2 + 2H_2O \qquad (6)$$

The resulting solution was evaporated on a water bath until dry. The dish containing the dry residue was then cooled in a cooling mixture (ice : table salt = 3 : 1) and dissolved in a 25% ammonia solution that had also been pre-cooled in the same cooling mixture. After a short period in the cooling mixture, crystallization of hexaammine nickel(II) bromide occurred:

$$NiBr_2 + 6NH_3 \rightarrow [Ni(NH_3)_6]Br_2$$

The purple crystals were separated by filtration, washed with a small amount of diluted ammonia, and dried in a vacuum desiccator.

Both synthesized compounds were stored in well-sealed containers, as exposure to air leads to ammonia loss from the complex over time.

2.3. Characterization Methods

The morphology of the samples was examined using Tescan Vega III Easyprobe scanning electron microscope (Tescan, Brno, Czech Republic) equipped with a tungsten filament, operated at an accelerating voltage of 10 kV. Samples were mounted on holders using self-adhesive carbon tape and sputter-coated with a gold–palladium alloy using Quorum SC 7620 sputter coater (Quorum Technologies, Laughton, UK). The chemical composition and elemental distribution of the synthesized compounds were analyzed by energy-dispersive X-ray spectroscopy (EDS) using Bruker Quantax system (Bruker, Billerica, MA, USA).

Phase identification was performed by X-ray powder diffraction (XRD) analysis using Rigaku Miniflex 600 diffractometer (Rigaku, Tokyo, Japan) with CuKα radiation. Data were collected in the 2θ range of 10° to 70°, with a step size of 0.01° and a scan speed of $10° \cdot min^{-1}$.

In order to compare the chemical bonding in both prepared compounds, FTIR analyses were conducted on Bruker Vertex 70 spectrometer (Bruker Optics, Karlsruhe, Germany) in attenuated total reflectance (ATR) mode, using samples pressed onto a diamond crystal. Spectra were recorded in the range of 400–4000 cm^{-1} with a resolution of 2 cm^{-1}, and the final spectrum represents the average of 32 scans.

Differential thermal analysis (DTA) was performed to gain insight into the course of thermally induced decomposition processes of the prepared compounds. DTA was carried out using NETZSCH STA 409 thermal analyzer (NETZSCH, Selb, Germany). Approximately 50 mg of the sample were placed in an α-Al_2O_3 crucible, which was also used as the reference material. The sample was heated from room temperature to 650 °C at a rate of 10 $°C \cdot min^{-1}$ under an air flow of 30 $cm^3 \cdot min^{-1}$. Differential scanning calorimetry (DSC) was performed on LINSEIS DSC PT 1600 instrument (LINSEIS, Selb, Germany) under the same conditions: approximately 50 mg of the sample were put in an α-Al_2O_3 crucible, heated from room temperature to 650 °C at 10 $°C \cdot min^{-1}$ in an air flow.

3. RESULTS AND DISCUSSION

To gain insight into the morphology of the obtained samples, SEM analysis was performed (**Figure 2**). Both samples are polydisperse, containing particles ranging from submicron sizes and agglomerates up to several micrometers in size. Such size distribution is a consequence of multiple nucleation and growth events during the

synthesis since uniform conditions are hard to achieve in the course of exothermal process. Octahedral units are visible in the micrographs of both samples, which is consistent with the cubic structure of the investigated hexaammine halides since the surfaces of the octahedra correspond to (111) planes of hexamine nickel halide cubic structures. The presence of octahedral units in the microstructure of hexaammine metal halides has also been reported in the literature (Rejitha 2010).

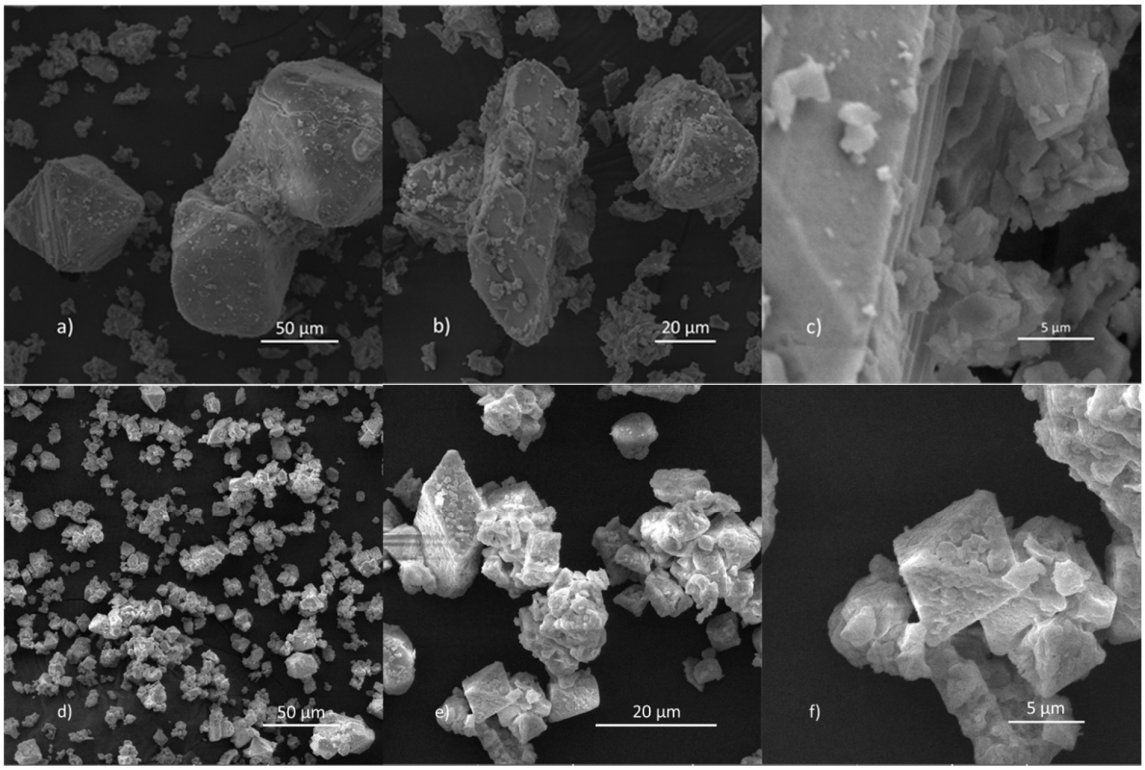

Figure 2. *SEM micrographs of the samples: a)-c) $[Ni(NH_3)_6]Cl_2$ and d)-f) $[Ni(NH_3)_6]Br_2$*
Elemental distribution mapping of the samples shown in ***Figure 3*** *indicates a uniform distribution, consistent with the monophasic nature of the material. However, the data for nitrogen are not entirely reliable, as elements with lower atomic numbers, such as nitrogen, cannot be accurately quantified using this method.*

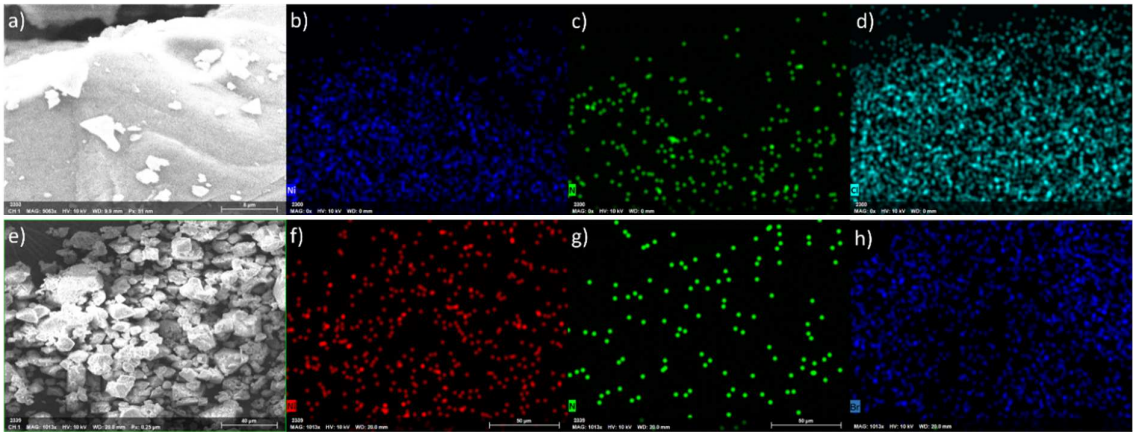

Figure 3. *EDS elemental distribution maps of the samples: a) - d) $[Ni(NH_3)_6]Cl_2$ and e) - h) $[Ni(NH_3)_6]Br_2$. Where b) and f) show Ni, c) and g) show N, d) shows Cl and h) shows Br distribution in samples.*

Comparison of the XRD patterns of the investigated samples shown in **Figures 4a** and **4b** with literature data (Breternitz 2016), (Rejitha 2010), (Eßmann et al. 1996), (Müller 1974) confirms that the synthesized samples are pure $[Ni(NH_3)_6]Cl_2$ (ICDD PDF No. 24-803) and $[Ni(NH_3)_6]Br_2$ (ICDD PDF No. 24-802). The samples are isostructural and their crystal structure adopts a space group Fm-3m (**Figure 5**) with most prominent peaks from (110), (200), (222) and (400) planes. Reflections from equivalent planes for $[Ni(NH_3)_6]Br_2$ appear at slightly lower

angles compared to $[Ni(NH_3)_6]Cl_2$, due to the larger ionic radius of the Br^- ion (196 pm) relative to the Cl^- ion (181 pm). For example, the (110) peak of $[Ni(NH_3)_6]Br_2$ appears at an angle 0.6 °(2θ) greater than the same peak of $[Ni(NH_3)_6]Cl_2$. The diffraction peaks are relatively sharp, indicating that the crystallites are fairly large, which is consistent with the SEM analysis results.

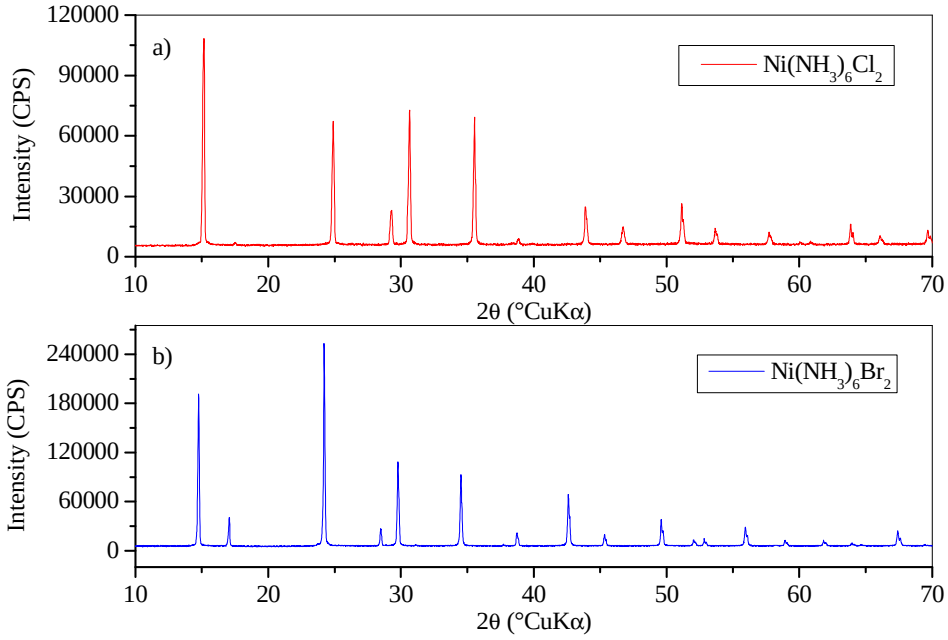

Figure 4. *XRD patterns of samples: a) $[Ni(NH_3)_6]Cl_2$ and b) $[Ni(NH_3)_6]Br_2$*

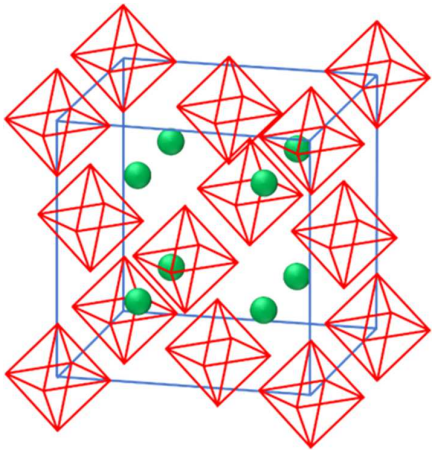

Figure 5. *Structural representation of $[Ni(NH_3)_6]Cl_2$ and $[Ni(NH_3)_6]Br_2$. The compounds are composed of $[Ni(NH_3)_6]^{2+}$ octahedra (shown in red, as in **Figure 1**) and halide anions (represented as green spheres)*

Both FTIR spectra shown on **Figure 6a** and **6b** are very similar, with only minor shifts in band positions. The band with a maximum at 3348 cm^{-1} for $[Ni(NH_3)_6]Cl_2$ and at 3329 cm^{-1} for $[Ni(NH_3)6]Br_2$ results from the overlap of the asymmetric (ν_a) and symmetric (ν_s) N–H stretching vibrations (Breternitz 2016), (Eßmann et al. 1996), (Müller 1974). The bands with maxima at approximately 1600 and 1170 cm^{-1} for $[Ni(NH_3)_6]Cl_2$, and at ~1593 and ~1184 cm^{-1} for $[Ni(NH_3)_6]Br_2$, originate from the asymmetric (δ_a) and symmetric (δ_s) bending vibrations of the H–N–H group, respectively. The band observed at 680 cm^{-1} for $[Ni(NH_3)_6]Cl_2$ and 670 cm^{-1} for $[Ni(NH_3)_6]Br_2$ can be attributed to the NH_3 rocking vibration (ρ) (Breternitz 2016), (Eßmann & Mockenhaupt 1996).

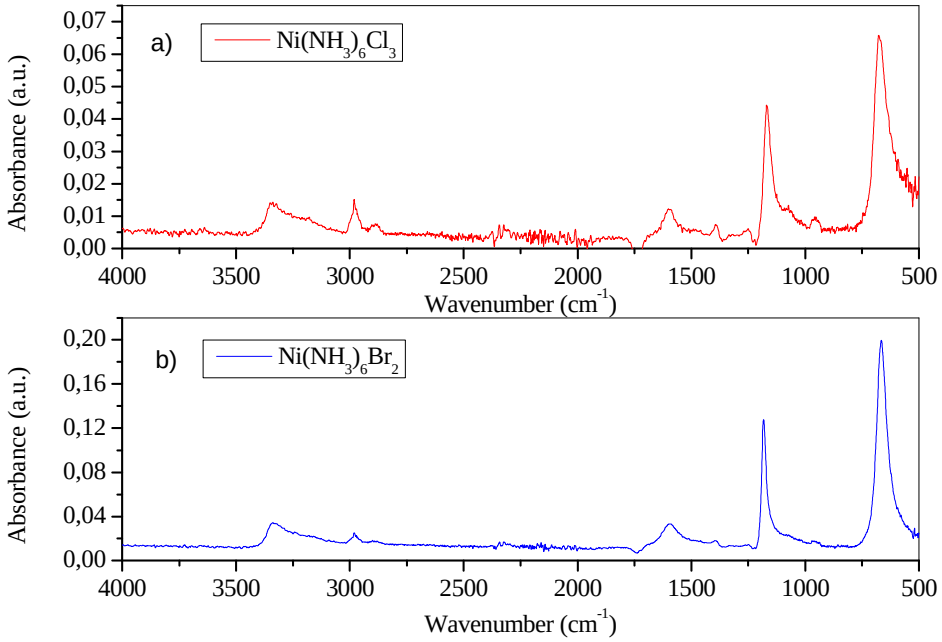

Figure 6. *FTIR spectra of samples: a) $Ni(NH_3)_6Cl_2$ and b) $Ni(NH_3)_6Br_2$*

The results indicate that the stretching and rocking vibrations are shifted to lower wavenumbers in $[Ni(NH_3)_6]Br_2$ compared to $[Ni(NH_3)_6]Cl_2$, whereas the bending vibrations do not show a systematic shift. The shift of the rocking vibration toward lower wavenumbers is attributed to the weakening of hydrogen bonding interactions with the halide (Kojima 2020), (Yamane 2014), (Fujita 1956).

Figures 7 and **8** show the TGA, DTG, and DSC curves obtained at a heating rate of 10 °C·min^{-1} for the samples $[Ni(NH_3)_6]Cl_2$ (**Figure 7**) and $[Ni(NH_3)_6]Br_2$ (**Figure 8**). At this heating rate, both samples exhibit two distinct mass loss steps, as indicated by the DTG curves. The onset temperature of the decomposition process is difficult to determine precisely; therefore, the temperatures of the DTG peak maxima are reported instead, as they approximately correspond to the temperatures at which the rate of mass loss is the highest.

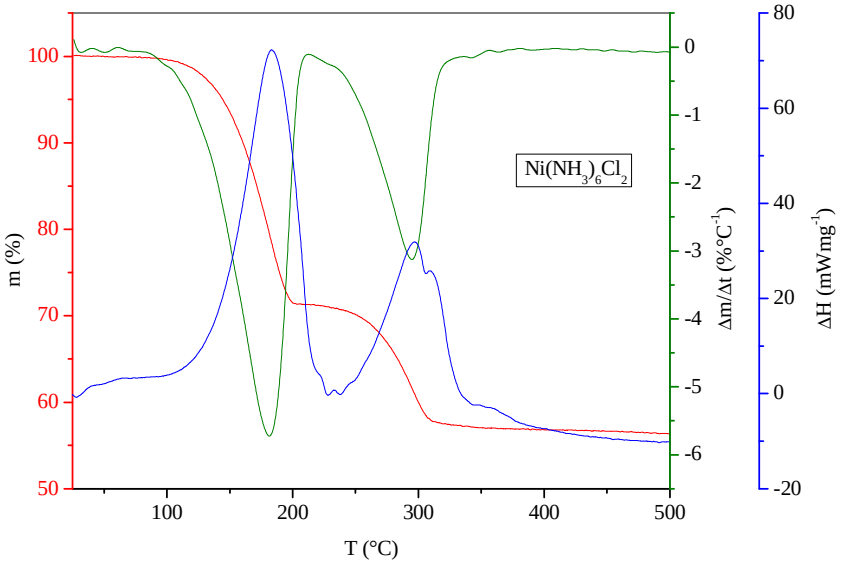

Figure 7. *TGA, DTG, and DSC curves of the sample $[Ni(NH_3)_6]Cl_2$*

For the $[Ni(NH_3)_6]Cl_2$ sample, the DTG peak maxima occur at 182 °C and 296 °C. The corresponding endothermic peaks observed in the DSC curve align well with the DTG peaks. However, a shoulder is visible on the right side of the second DSC peak, with a local maximum at 309 °C. Mass losses calculated from the TGA

curve are 28.7 % and 14.4 %, respectively. Theoretically, the loss of four NH_3 molecules from $[Ni(NH_3)_6]Cl_2$ corresponds to a mass loss of 29.4 %, and the loss of two molecules corresponds to 14.7 %. The experimental values match the theoretical ones reasonably well, indicating that the first mass loss step corresponds to the desorption of four NH_3 molecules. Considering the shoulder on the second DSC peak, it can be concluded that this step is followed by two separate desorption events, each involving the release of one NH_3 molecule.

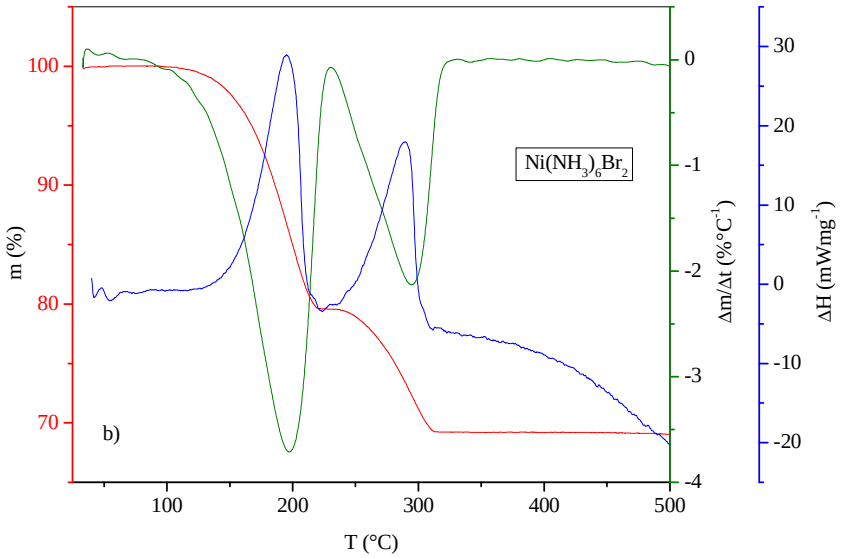

Figure 8. *TGA, DTG, and DSC curves of the sample $[Ni(NH_3)_6]Br_2$*

For the $[Ni(NH_3)_6]Br_2$ sample, the DTG peaks appear at 197 °C and 294 °C. The endothermic peaks in the DSC curve also align closely with the DTG maxima, although no shoulder is observed on the second DSC peak in this case. Mass losses calculated from the TGA curve are 20.4 % and 10.3 %, respectively. Theoretical calculations show that the loss of four NH_3 molecules corresponds to 21.3 %, and the loss of two molecules to 10.6 %. Once again, the agreement between experimental and theoretical values is good, supporting the conclusion that the first step involves the desorption of four NH_3 molecules, and the second step two NH_3 molecules from $[Ni(NH_3)_6]Br_2$. Minor discrepancies may be attributed to partial ammonia loss during sample storage or incomplete desorption during analysis.

Most amino metal halide complexes have stoichiometry less favourable for ammonia or hydrogen storage, i.e. contain fewer ammonia molecules, e.g. $[Mn(NH_3)_2]Cl_2$, $[Fe(NH_3)_3]Cl_2$ and $[Zn(NH_3)_4]Cl_2$. $[Ni(NH_3)_6]Cl_2$ and $[Ni(NH_3)_6]Br_2$ have a much more suitable stoichiometry and thus represent a promising class of materials capable of reversibly storing significant amounts of ammonia or hydrogen.

Literature reports indicate that the thermal decomposition of both $[Ni(NH_3)_6]Cl_2$ and $[Ni(NH_3)_6]Br_2$ proceeds in three steps (Breternitz 2016), (George 1963). The formation of the monoammine intermediate is more readily detected at higher heating rates. This behavior is attributed to kinetic effects: regardless of the heating rate, the diamine first decomposes to the monoammine, which then decomposes to the anhydrous halide. However, at lower heating rates, the decomposition of the ammine is slower than that of the monoammine, making the monoammine decomposition step unobservable by thermal analysis. Only at higher heating rates does the decomposition of the ammine proceed at a comparable rate to that of the monoammine, allowing detection of both steps (George 1963).

The decomposition temperatures correspond well with data given in literature. (Breternitz, 2016) While the second decomposition peak occurs at similar temperatures for both samples, the first peak appears approximately 15 °C lower for $[Ni(NH_3)_6]Cl_2$ compared to $[Ni(NH_3)_6]Br_2$. This difference may be related to the binding energy of NH3 to surrounding ions, which appears to be slightly higher in $[Ni(NH_3)_6]Br_2$ (Lysgaard 2012). Alternatively, the higher desorption temperature observed for $[Ni(NH_3)_6]Br_2$ could result from differences in the lattice energy of $NiCl_2$ and $NiBr_2$. Given that the ionic radius of Cl^- is smaller than that of Br^-, according to the Kapustinskii equation, the lattice energy of $NiCl_2$ should be higher (i.e., more negative) than that of $NiBr_2$. Consequently, from a thermodynamic perspective, the decomposition of $[Ni(NH_3)_6]Cl_2$ is slightly more favourable, resulting in its decomposition at a lower temperature (Jones 2013).

It should be stressed that the usage of hexamine nickel(II) halides poses a certain threat to the environment and human health. Nickel could harm aquatic life and enter the food chain, while ammonia can cause eutrophication and be toxic for life in aquatic systems. Therefore, a careful management of waste and emissions is required (Genchi 2020), (Edwards 2024).

4. CONCLUSION

Hexaammine complexes of nickel chloride and nickel bromide, $[Ni(NH_3)_6]Cl_2$ and $[Ni(NH_3)_6]Br_2$, were synthesized from the corresponding nickel halides and ammonia. The prepared particles are polydisperse, agglomerated, and exhibit characteristic octahedral morphology. The samples consist exclusively of pure, well-crystallized hexaammine complexes. Both compounds are isostructural and crystallize in the K_2PtCl_6-type structure with space group Fm-3m. $[Ni(NH_3)_6]Br_2$ exhibits slightly weaker nitrogen–metal coordination and weaker hydrogen bonding with the halide.

Thermal analysis showed that under the applied experimental conditions, ammonia release from $[Ni(NH_3)_6]Cl_2$ occurs in three steps: initially, four NH_3 molecules are released, followed by one molecule in each of the subsequent two steps. In contrast, the decomposition of $[Ni(NH_3)_6]Br_2$ proceeds in two steps, involving the loss of four and then two NH_3 molecules. This difference is attributed to the kinetic parameters of the desorption process. The first desorption peak occurs at a slightly lower temperature for the $[Ni(NH_3)_6]Cl_2$ sample compared to $[Ni(NH_3)_6]Br_2$, which is ascribed to thermodynamic factors.

Nickel dihalide ammines represent a promising class of materials capable of reversibly storing significant amounts of ammonia or hydrogen. They are readily synthesized and exhibit thermal decomposition at moderate temperatures.

5. ACKNOWLEDGMENTS

M. S. would like to gratefully acknowledge the hospitality of the Faculty of Chemical Engineering and Technology, University of Zagreb, Croatia. The aegis of University of Zagreb is gratefully acknowledged.

6. REFERENCES

Aziz M, TriWijayanta A, Nandiyanto A B D (2020) Ammonia as effective hydrogen storage: A review on production, storage and utilization, Energies, 13, 3062.

Berdiyeva P, Karabanova A, Grinderslev J B, et al. (2020) Synthesis, structure and NH_3 sorption properties of mixed $Mg_{1-x}Mn_x(NH_3)_6Cl_2$ ammines, Energies, 13, 2746.

Bialy A, Jensen P B, Blanchard D, Vegge T, Quaade U J (2015) Solid solution barium–strontium chlorides with tunable ammonia desorption properties and superior storage capacity, J. Solid State Chem., 221, 32–36.

Breternitz J, Vilk Y E, Giraud E, Reardon H, Hoang T K A, Godula-Jopek A, Gregory D H (2016) Facile uptake and release of ammonia by nickel halide ammines, ChemSusChem, 9, 1312 – 1321.

Edwards T M, Puglis H J, Kent D B, Duran J L, Bradshaw L M, Farag A M (2024) Ammonia and acquatic ecosystems – a review of global sources, biogeochemical cycling, and effect on fish, Sci. Total Environ., 907, 167911.

Eßmann R, Kreiner G, Niemann A, Rechenbach D, Schmieding A, Sichla T, Zachwieja U, Jacobs H (1996) Isotype Strukturen einiger Hexaamminmetall(II)-halogenide von 3d-Metallen: $[V(NH_3)_6]I_2$, $[Cr(NH_3)_6]I_2$, $[Mn(NH_3)_6]Cl_2$, $[Fe(NH_3)_6]Cl_2$, $[Fe(NH_3)_6]Br_2$, $[Co(NH_3)_6]Br_2$ und $[Ni(NH_3)_6]Cl_2$. Z. Anorg. Allg. Chem., 622, 1161–1166.

Eßmann R, Mockenhaupt C (1996) Influence of coordination on N-H ⋯ X− hydrogen bonds. Part II. $Zn(NH_3)_2Br_2$ and $Ni(NH_3)_2X_2$ (X is Cl^- and Br^-), Spectrochim. Acta**,** A52, 1897–1901.

Freeman N Z, Zong H, Xie P, Wang C (2023) Catalytic cracking of ammonia toward carbon-neutral liquid fuel, Curr. Opin. Green Sustain. Chem., 44, 100860.

Fujita J, Nakamoto K, Kobayashi M (1956) Infrared Spectra of Metallic Complexes. I. The Effect of Coördination on the Infrared Spectra of Ammine, Rhodanato and Azido Complexes, J. Am. Chem. Soc., 78, 3295 –3297.

Genchi G A, Carocci A, Lauria G, Sinicropi M S, Catalano A (2020) Nickel: Human health and environmental toxicology, Int. J. Environ. Res. Public Health, 17, 697.

George T D, Wendlandt W W (1963) The thermal decomposition of metal complexes—II Some ammine and ethylenediamine complexes of nickel (II). J. Inorg. Nucl. Chem., 25, 395–405.

Hodorowicz S A, Eick H A (1982) Phase relationships in the system SrBr2 SrCl2, J. Solid State Chem. 43, 271–277.

Jacobsen H S, Hansen H A, Andreasen J et al. (2007) Nanoscale structural characterization of $Mg(NH_3)_6Cl_2$ during NH_3 desorption: An in situ small angle X-ray scattering study, Chem. Phys. Lett., 441, 255–260.

Jones M O, Royse D M, Edwards P P, David W I F (2013) The structure and desorption properties of the ammines of the group II Halides, Chem. Phys., 427, 38–43.

Klerke A, Christensen C H, Nørskov J K, Vegge T (2008) Ammonia for hydrogen storage: challenges and opportunities, J. Mater. Chem., 18, 2304–2310.

Klopčič N, Grimmer I, Winkler F, Sartory M, Trattner A (2023): A review on metal hydride materials for hydrogen storage, J. Energy Storage, 72B, 108456.

Kojima Y, Yamaguchi M (2020) Ammonia storage materials for nitrogen recycling hydrogen and energy carriers, Int. J. Hydrogen Energy, 45, 10233-10246.

Liu C Y, Aika K-I (2004) Ammonia absorption on alkaline earth halides as ammonia separation and storage procedure, Bull. Chem. Soc. of Jpn., 77, 123-131.

Lysgaard S, Ammitzbøll A L, Johnsen R E, Norby P, Quaade U J, Vegge T (2012) Resolving the stability and structure of strontium chloride amines from equilibrium pressures, XRD and DFT, Int. J. Hydrog. Energy, 37, 18927–18936.

Mandal T K, Gregory D H (2009): Hydrogen storage materials: present scenarios and future directions, Ann. Rep. Prog. Chem. Sect. A, 105, 21–54.

Müller A, Schmidt K H, Vandrish G (1974) Vibrational spectra and pseudo-exact force constants of $[Ni(NH_3)_6]^{2+}$, $[Zn(NH_3)_4]^{2+}$, and $[Zn(CN)_4]_2$- with 58Ni/62Ni, 64Zn/68Zn and H/D isotopic substitution, Spectrochim. Acta, A30, 651-663.

Müller D, Knoll C, Gravogl G, Jordan C, Eitenberger E, Friedbacher G, Artner W, Welch J M, Werner A, Harasek M, Miletich R, Weinberger P. (2021) Medium-temperature thermochemical energy storage with transition metal ammoniates – A systematic material comparison, App. Energy, 28, 116470.

Ni M, Leung D Y C, Leung M K H (2008) An improved electrochemical model for the NH_3 fed proton conducting solid oxide fuel cells at intermediate temperatures, J. Power Sources, 185, 233–240.

Reardon H, Hanlon J M, Grant M, Fullbrook I, Gregory D H (2012) Ammonia uptake and release in the MnX_2–NH_3 (X = Cl, Br) systems and structure of the $Mn(NH_3)_nX_2$ (n = 6, 2) ammines, Crystals, 2, 193-212.

Rejitha K S, Ichikawa T, Mathew S (2010) Thermal decomposition studies of $[Ni(NH_3)_6]X_2$ (X = Cl, Br) in the solid state using TG-MS and TR-XRD, J. Therm. Ana.l Calorim., 103, 515–523.

Sørensen B (2005) Hydrogen and Fuel Cells: Emerging Technologies and Applications, 2nd ed. Academic Press: New York, USA, pp. 5-94.

Straub A, Dorneanu B, Arellano-Garcia H (2023) Towards a novel concept for solid energy storage, Comput. Aided Chem. Eng., 52, 2963.

von Colbe J B, Ares J-R, Barale J, Baricco M, Buckley C, Capurso G, et al. (2019) Application of hydrides in hydrogen storage and compression: achievements, outlook and perspectives, Int. J. Hydrogen Energy, 44, 7780-7808.

Yamane A, Shimojo F, Ichikawa T, Kojima Y (2014) Cation/anion dependence of metal ammine borohydrides/chlorides studied by ab initio calculations, Comput. Theor. Chem., 1039C, 71-74.